

Height-resolved variability of midlatitude tropospheric water vapor measured by an airborne lidar

Lucas Fischer,¹ Christoph Kiemle,² and George C. Craig¹

Received 14 December 2011; revised 23 February 2012; accepted 24 February 2012; published 20 March 2012.

[1] Free tropospheric water vapor variability, measured by airborne lidar over Europe during summertime, is analyzed at altitudes from 2 km to 10 km. Horizontal structure functions of specific humidity were computed and show power-law scaling between about 10 km to 100 km in range. The second-order structure function shows scaling exponents equivalent to spectral slopes that vary from around $5/3$ in the lower troposphere to 2 at upper levels. More specifically humidity smoothness typically increases with height, while intermittency decreases. A classification of the data according to whether the series occurred above or below the level of nearby convective cloud tops gives a separation of the scaling exponents in the two air masses. The results are consistent with a water vapor distribution determined at upper levels by a downscale cascade of variance by advective mixing, but increasingly influenced at lower levels by local injection of humidity by moist convection. **Citation:** Fischer, L., C. Kiemle, and G. C. Craig (2012), Height-resolved variability of midlatitude tropospheric water vapor measured by an airborne lidar, *Geophys. Res. Lett.*, 39, L06803, doi:10.1029/2011GL050621.

1. Introduction

[2] Tropospheric water vapor plays an important role in the climate system through its direct influence on the radiation budget, and through its influence on dynamical processes, such as cumulus convection [Sherwood *et al.*, 2010]. The complex dynamics of water vapor in the free troposphere includes a range of source and sink processes from convective clouds on the kilometre scale to cloud systems associated with motions on scales of a thousand or more kilometres, as well as advection of water vapor as a passive tracer outside of clouds [Emanuel and Pierrehumbert, 1996]. While large-scale advection of water vapor is well represented in general circulation models, the simulations are heavily dependent on the parameterizations of small scale processes. Traditionally, deterministic parameterization schemes are used to provide an average description of the effects of unresolved processes such as cumulus convection on the larger scales. However, Tompkins and Berner [2008] and Zhang *et al.* [2003] investigated the moisture-convection interaction and found out that a lack of knowledge of humidity fluctuations on scales smaller than the mesoscale model grid leads to errors in the development of deep convection and increases the prediction uncertainty.

This problem can be addressed with the use of stochastic parameterisations that attempt to explicitly describe variability near the model grid length [e.g., Craig and Cohen, 2006; Kärcher and Burkhardt, 2008; Plant and Craig, 2008]. However, the design and testing of such schemes depends on an accurate characterization of small-scale variability in nature, and subgrid-scale humidity fluctuations have not yet been empirically explored throughout the troposphere in detail [Pressel *et al.*, 2010].

[3] Scale dependencies of the variability of water vapor have so far been investigated in the course of only three aircraft studies [Nastrom *et al.*, 1986; Cho *et al.*, 2000; Kahn *et al.*, 2011]. In each of these studies the analysis is based on *in situ* measurements, i.e., measuring only one height in a given flight segment. Table 1 shows the average results of each of these studies, with their standard deviations where available. Nastrom *et al.* [1986] obtained a variance spectrum with a slope ($k^{-\beta}$) of $\beta = 5/3$ in the upper troposphere. Cho *et al.* [2000] separated the atmosphere into three different regimes - marine boundary layer (a), tropical free troposphere (b), and extratropical free troposphere (c) - and obtained different spectral slopes (a = 1.46, b = 1.63, c = 1.79). By using structure functions Cho *et al.* [2000] further found that the tropical free troposphere has a more intermittent water vapor field than the extratropical free troposphere. Kahn *et al.* [2011] detected increasing spectral slopes with height, finding a minimum of 1.58 at 1.5 km and a maximum of 1.90 at heights above 3 km.

[4] A spectral slope of $5/3$ for both kinetic energy and the variance of a passive tracer (e.g., water vapor in the absence of clouds) is predicted by the classical Obukhov-Corrsin theory of three-dimensional homogeneous turbulence [Corrsin, 1951; Obukhov, 1949]. While this is not likely to be a correct description of the atmosphere on scales of tens or hundreds of kilometres, a $5/3$ slope in kinetic energy may also occur through gravity waves, or through upscale transfer from a small-scale source of variance such as cumulus convection [Vallis *et al.*, 1996; Xu *et al.*, 2011]. Furthermore, as noted by Shraiman and Siggia [2000], the statistical properties of passive scalar turbulence are decoupled from those of the underlying velocity field, with the consequence that a deviation from the classical downscale cascade of the velocity field can be expected. A steeper spectral slope is connected to the fact that large-scale motions in a turbulent velocity field exert a considerable influence on the passive scalar behavior [Zilberman *et al.*, 2008], leading, for example, to abrupt gradients associated with fronts [Nastrom *et al.*, 1986]. The range of values shown in Table 1 suggests that different mechanisms dominate the production of water vapor variance in the different data sets. Slopes steeper than $5/3$ suggest the importance of downscale transfers of scalar variance, but a slope of $5/3$ could also be a consequence of upscale transfers.

¹Institute of Meteorology, Ludwigs-Maximilians University, Munich, Germany.

²Institute of Atmospheric Physics, Deutsches Zentrum für Luft- und Raumfahrt, Oberpfaffenhofen, Germany.

Table 1. Average Scaling Exponents $\zeta_2 = \beta - 1$ of the Second-Order Structure Function of Moisture Time Series Measured During Aircraft Studies as a Function of Height h

Scaling [km]	Nastrom 8–500	Cho 0.05–100	Kahn 10–100	This Study 10–100
$h < 1.5$		0.46 ± 0.13	0.62	
$h < 3.0$			0.80	0.63 ± 0.17
$h > 3.0$		0.79 ± 0.17	0.90	0.81 ± 0.31
$h > 10.0$	0.66			

Identifying the physical mechanisms responsible for the statistics of water vapor variability in different parts of the atmosphere is a key issue in development of parameterisations of cloud processes, but is made difficult by the relative scarcity of high-resolution data.

[5] Here we present for the first time a statistical analysis of a tropospheric water vapor data set obtained from airborne lidar. This instrument provides vertical cross sections of water vapor mixing ratio at high spatial resolution, enabling the calculation of height-resolved spatial statistics including structure functions up to the fifth order. The results will be compared with previous studies, and a simple attempt is made to relate them to the meteorological conditions at different levels in the atmosphere.

2. Data and Method

[6] We use data from the COPS/ETReC 2007 (Convective and Orographically-induced Precipitation Study/European THORPEX Regional Campaign) field experiment conducted from June to August 2007. The overall mission was the study of key processes leading to convection initiation and modification of precipitation by orography. With a DIAL (Differential Absorption Lidar), which was installed nadir-pointing on board the DLR-Falcon research aircraft, two-dimensional measurements of the water vapor mixing ratio were taken during a total of 14 flights. A DIAL sends short and spectrally narrow laser pulses into the atmosphere at a wavelength tuned to the centre of a molecular water

vapor absorption line. The water vapor density can be derived from the difference in absorption between this ‘on-line’ and another ‘off-line’ non-absorbed laser pulse as function of distance from the lidar with an accuracy of a few percent [Kiemle *et al.*, 2011].

[7] The DLR-Falcon flew over middle and south-west Europe, between 41–49°N and 7.5°W–10°E. Six of the 14 flights had to be removed due to low lidar signals or large data gaps caused by clouds, aircraft turns or lidar adjustment phases. After horizontal averaging to a resolution of 2–3 km to obtain a high signal to noise ratio, and linear interpolation over small data gaps, we were able to investigate 8 flights with a length of 225 km to 700 km and a vertical extent from 2.0 km to 9.8 km (most flight segments have a length of 300 km and a vertical range of about 4 km). We estimated the signal to noise ratio using a lagged autocorrelation method to separate instrumental noise from atmospheric variability [Kiemle *et al.*, 1997]. The average statistical uncertainty over all 8 flights is about 3% and shows no systematic height dependency, since the usual lidar signal decreasing with range is compensated here by aerosol and water vapor densities that increase towards the ground. The boundary layer is not included, because this work is more focused on convective and advective rather than turbulent mixing and transport of moisture. Given the vertical DIAL resolution of 200 m we analyzed a total of 98 time series from 8 flights, corresponding to a total length of about 38 000 km.

[8] Figure 1 (top left) shows two representative humidity time series at constant heights of 3.2 km (bottom) and 6.0 km (top), taken from a single flight segment. The two series clearly display differences in smoothness and spikiness. In order to quantify these visible differences by appropriate statistical parameters we use the structure function

$$S_q(r) = \langle |f(x+r) - f(x)|^q \rangle \quad (1)$$

for a signal $f(x)$ at lag r and order q , where $\langle \dots \rangle$ represents an ensemble average, meaning that for every lag r the arithmetic mean is computed over all possible pairs of the absolute

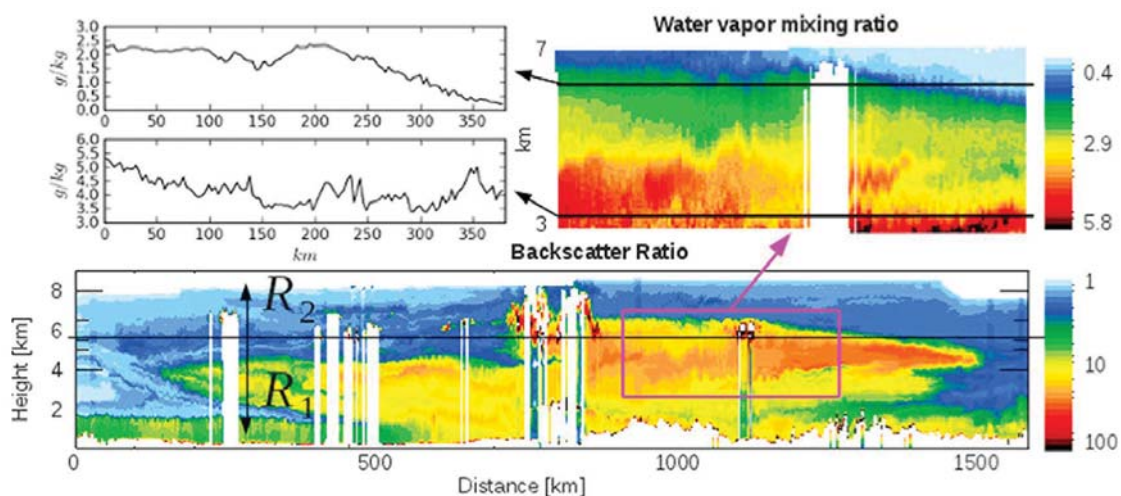


Figure 1. (top left) Representative specific humidity data samples from August 1 2007 (top) at 6.0 km and (bottom) at 3.2 km height; and lidar measurements of (top right) specific humidity (g/kg) for the analyzed 370 km flight segment; and (bottom) atmospheric backscatter ratio at 1064 nm wavelength for the whole flight. The black horizontal line at 5.7 km height marks the level of cloud base. R_1 and R_2 indicate the two air mass regimes defined in section 3.1.

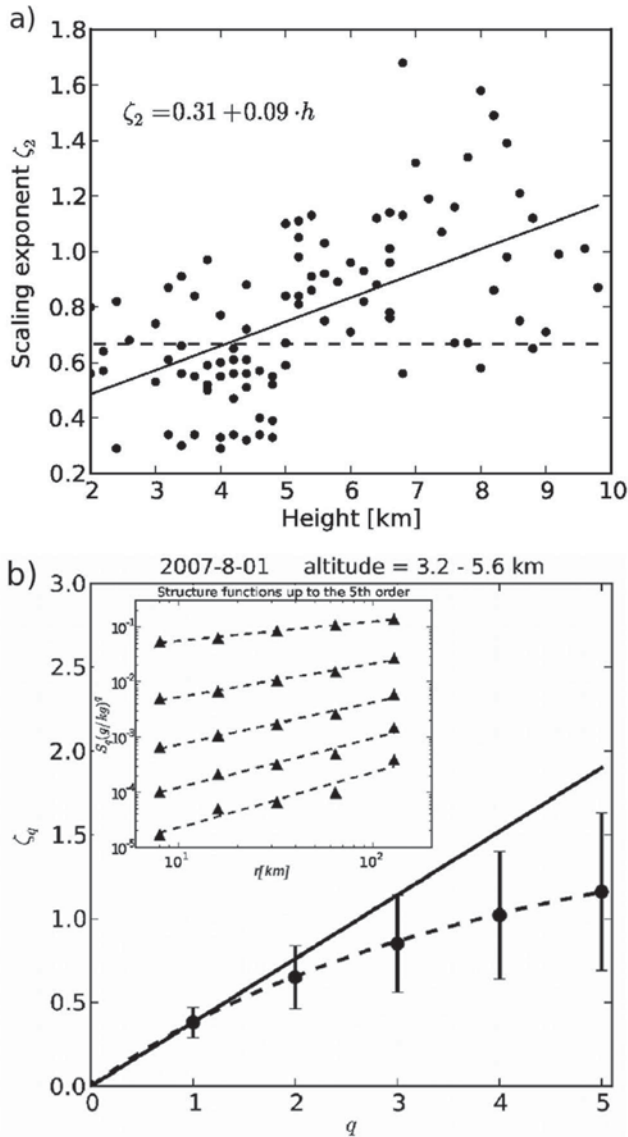


Figure 2. (a) Scaling exponent ζ_2 versus height for 98 segments from 8 flights during the COPS campaign. The solid line is computed by a least-squares regression with a fit parameter uncertainty of 0.013; the dashed line represents $\beta = 5/3$. (b) Structure functions up to the 5th order at 3.2 km height (inset). The order increases in unity steps from top to bottom. Straight lines are fitted to the structure functions from $r = 8$ km to $r = 120$ km (triangles). The average slopes calculated from the fits are plotted versus order q for twelve 370 km flight segments from 3.2–5.6 km height (main). The dashed curve is calculated by equation (4) (see text). The error bars are the standard deviations; the solid line represents hypothetical monofractal behaviour for comparison.

difference in water vapor mixing ratio within a flight segment, similar to *Davis et al.* [1994] and *Marshak et al.* [1997]. The main interest in structure functions is to quantify how they scale with lag r . Power-law scaling satisfies the relation

$$S_q(r) \propto r^{\zeta_q} \quad (2)$$

where the exponent ζ_q describes how the q th-order structure function scales with r . The scaling exponent of the first-order structure function ζ_1 , often called Hurst exponent or ‘roughness’, characterizes the nonstationarity of the data [*Marshak et al.*, 1997]. The range of ζ_1 is from zero to one, with values near zero characterizing rough, nearly stationary signals and values near one characterizing smooth, nonstationary signals [*Tuck et al.*, 2003].

[9] The second-order structure function S_2 is well known because of its Fourier duality with the power spectrum. Under the assumption that power-law relations are satisfied for all encompassed scales a relation between the spectral exponent β and the scaling exponent of the second-order structure function ζ_2

$$\beta = \zeta_2 + 1 \quad (3)$$

can be derived [*Lewis et al.*, 2004]. We find power-law relations on scales between 10 and 100 km (cf. Table 1). Fourier spectra are insufficient since they only fully reproduce stationary time series. Here however, two water vapor fields with identical second-order statistics may still display very different variability. On the other hand structure functions of higher order can give additional information [*Marshak et al.*, 1997]. Indeed, only in the case of so-called ordinary scaling (constant ratio ζ_q/q), do the structure functions provide the same information about the signal as the power spectrum. If the structure functions of higher order show anomalous scaling (ζ_q/q variable), the deviation from linear (ordinary) scaling describes the degree of intermittency, with larger deviations from linear scaling indicating increased intermittency [*Pierrehumbert*, 1996].

3. Results

3.1. Height Dependency of the First- and Second-Order Statistics of Moisture Variability

[10] First- and second-order structure functions and scaling exponents ζ_1 and ζ_2 have been calculated for the 98 moisture time series described above. Figure 2a shows the values of ζ_2 plotted against height. The exponent varies from 0.29 ± 0.10 to 1.68 ± 0.10 , with a tendency towards higher values at higher heights. The individual uncertainties vary between ± 0.05 and ± 0.15 and show no height dependency. Transforming the exponents to spectral slopes (equation (3)), gives a range of $\beta = 1.29 - 2.68$. As listed in Table 1, the few existing aircraft studies of water vapor spectra have found approximate scaling exponents β ranging from 1.46 to 1.90 [*Nastrom et al.*, 1986; *Cho et al.*, 2000; *Kahn et al.*, 2011]. Averaging the results of the present study for heights below and above 3 km, give exponents of 1.63 and 1.81, respectively, which is broadly consistent with the earlier work. Interestingly the values in the lower levels scatter about the theoretical $\beta = 5/3$ predicted for homogeneous turbulence, or alternatively upscale transfer from convection, while the slope at upper levels is steeper, pointing to downscale influence.

[11] As noted in the introduction, various explanations have been suggested for the change of spectral slope with height. Here, the two dimensional lidar cross sections provide valuable additional information. For example, for the time series shown in Figure 1 (top left), a warm, moist air mass of Mediterranean origin was found below a height of

Table 2. Characteristics and Statistical Properties of the Two Regimes Found in the Dataset of the COPS Campaign^a

R_1 Date	L (km)	h (km)	N	ζ_1	ζ_2	ζ_∞
18.07.	225	3.4–4.8	5	0.41	0.72	3.6
19.07.	250	3.2–4.6	6	0.27	0.49	3.7
20.07.	340	3.0–5.0	9	0.35	0.64	5.4
26.07.	360	2.0–2.4	3	0.31	0.57	3.3
30.07.	500	2.0–4.0	8	0.33	0.58	2.7
01.08.	370	3.2–5.6	12	0.39	0.66	3.0
Averages				0.36 ± 0.11	0.61 ± 0.19	3.6 ± 3.2
R_2 Date	L (km)	h (km)	N	ζ_1	ζ_2	ζ_∞
08.07. I	700	6.6–9.8	15	0.65	1.19	8.6
08.07. II	300	4.2–6.0	10	0.47	0.86	5.2
18.07.	225	5.0–6.6	3	0.56	0.98	4.6
19.07.	250	4.8–9.0	16	0.40	0.75	7.8
20.07.	340	5.2–5.8	3	0.57	1.05	7.8
01.08.	370	5.8–7.0	8	0.55	1.01	6.2
Averages				0.53 ± 0.15	0.97 ± 0.25	6.7 ± 4.3

^a R_1 indicates height levels with dominating moist convective influences, R_2 indicates height levels with dry and cloud free air masses likely advected by the large-scale flow. L is the length of the time series, N is the number of time series.

5 km \pm 1 km. The boundary between this air mass and the air above is clearly visible in the lidar backscatter ratio (Figure 1, bottom). As seen in the backscatter and humidity cross sections in Figure 1, moist convection occurred in numerous times and places in the lower level air mass, penetrating to a stable layer at its upper boundary. Above the boundary, air of Atlantic origin can be found that shows substantially less small-scale variability, which is consistent with the observed steeper spectral slope of humidity variance. This pattern of two layers occurred frequently during the period of the COPS campaign, and has been examined in detail for the 1 Aug 2007 case study by *Schaefer et al.* [2010]. As an alternative to examining the change in structure functions with geometric height, we have attempted to classify the time series into two groups, characterized by whether or not they occurred in an air mass influenced by cumulus convection. The classification was performed by determining the cloud height from the lidar backscatter signal of the corresponding flight. The individual time series were assigned to the convectively influenced category (R_1) if located below that height, and to the second category (R_2) if above. By this method, 43 time series were assigned to R_1 , and 55 to R_2 . As shown in Table 2, the boundary between the two regimes occurred between 4 and 6 km in height during the COPS experiment.

[12] Table 2 shows first- and second-order scaling exponents (ζ_1 and ζ_2) for the two regimes for each of the 8 flights (note that both regimes were present in the same flight segment on only half of the flights.) The average Hurst exponent for the convective regime, $\zeta_1 = 0.36$, is smaller than for R_2 , where it takes the value 0.53. This indicates that the humidity time series at lower, more convective levels are rougher and have longer range correlations [*Tuck et al.*, 2003] than at higher heights. The two timeseries at heights of 3.2 km (bottom) and 6.0 km (top), shown as an example in Figure 1 (top left), clearly display these differences in smoothness.

[13] The difference in the second-order structure function exponent ζ_2 between the two regimes shows up clearly, with average values of 0.61 in the convectively-influenced region R_1 , and 0.97 in R_2 . The value in R_1 is close to the classical value of 2/3, corresponding to a spectral slope of 5/3, while the larger value in R_2 corresponds to a steeper slope.

3.2. Characterization of Atmospheric Processes by Higher Order Structure Functions

[14] Structure functions of higher orders are necessary to fully characterize nonstationary time series. The intermittency can be calculated from the variation of the scaling exponents ζ_q with q . Figure 2b (inset) shows a typical case of high intermittency in the lower troposphere (3.2 km) using the data of Figure 1 (top left). The log-log slopes (ζ_q) were calculated by a least-squares fit, as displayed in Figure 2b (inset). The dashed curve in Figure 2b (main) is calculated by an empirical two-parameter function introduced by *Pierrehumbert* [1996] which is as follows

$$\zeta_q = \frac{aq}{1 + a\frac{q}{\zeta_\infty}}. \quad (4)$$

We evaluated the parameters a and ζ_∞ by requiring equation (4) to match the data exactly at $q = 1$ and $q = 5$. The coefficient $a \approx \zeta_1$ measures smoothness and ζ_∞ measures multifractality or intermittency. $\zeta_\infty = \infty$ represents simple scaling, with decreasing values of ζ_∞ corresponding to larger probabilities that the field contains jump discontinuities [*Pierrehumbert*, 1996; *Lewis et al.*, 2004]. Intermittency describes the tendency of passive tracers to concentrate in localized, intermittent structures [*Shraiman and Siggia*, 2000; *Tuck et al.*, 2003]. By calculating the intermittency of the two humidity time series of Figure 1 (top left) we find $\zeta_\infty = 2.3$ at 3.2 km, and $\zeta_\infty = 7.9$ at 6.0 km. The former indicates strong and the latter weak intermittency, confirming the visual impression from Figure 1 (top left).

[15] Values of ζ_∞ for the complete data set are listed in Table 2, and again show a clear difference between the two regimes R_1 and R_2 . R_1 is characterized by lower values and thus higher intermittency than R_2 (3.6 vs. 6.7). The flight on 18 July is a potential outlier in Table 2, since the differences in intermittency between the two regimes was not so pronounced on that day. This is likely due to stratiform precipitation that occurred a few hours before the measurement time. The mean of ζ_∞ for R_1 of 3.6 lies between the values calculated for the tropical (2.3) and extratropical (4.7) troposphere by *Cho et al.* [2000], while the mean for R_2 is higher. A more precise comparison is difficult, since the values provided by *Cho et al.* [2000] are averaged throughout the free troposphere.

4. Conclusions

[16] Airborne DIAL water vapor measurements from eight flights on 7 days of the COPS experiment have been analyzed in order to characterize the variability of tropospheric humidity on length scales from 2 to 300 km. Structure functions of 98 time series of tropospheric water vapor fluctuations showed power law scaling between about 10 and 100 km. The scaling exponents ζ_1 , ζ_2 and intermittency (ζ_∞) are significantly dependent on height. Using the two dimensional lidar backscatter cross sections, we were able to

associate the change in variability statistics to an air mass boundary separating low-level air where cumulus convection was occurring from higher-level air above the convective cloud tops. The convectively influenced air masses, present at some level in 5 of the 8 flights, showed consistently shallower spectral slope (smaller ζ_2), greater roughness (smaller Hurst exponent ζ_1), and significantly higher intermittency (departure from mono-fractality shown by smaller ζ_∞).

[17] The value of the second-order structure function, $\zeta_2 = 0.61$ is consistent with the classical $-5/3$ spectral slope. Mechanisms for producing this slope have been proposed based on both downscale cascade of tracer variance, and upscale transfers from a small scale source such as convection. The higher order structure functions presented here, as well as the subjective classification of time series based on the presence of convection, provide strong evidence for a small-scale source of moisture variability. Note however that the analysis does not exclude the presence of downscale transfers of variance. On the other hand, theories for the steeper spectral slope found above the convectively-influenced air masses all rely on downscale transfers.

[18] It is worth noting that no scale break was observed. This is partly due to the relatively narrow range of scales present in the flight data, but the distinction between air masses is not fundamentally one of length scale and would not show up as a scale break in any case. It is probably not significant that the air mass boundary during the aircraft deployment in July 2007 consistently occurred at a height of around 5 km, and it will be interesting to compare this period with other data sets. Provided that the two regimes are taken into account, it appears that the structure function exponents provide a compact statistical description of moisture variability on scales just below the resolution of weather and climate models. This knowledge can be directly applied, for example, to the design of stochastic or pdf-based parameterizations for clouds and convection by using the spectral information to construct realisations of the small-scale moisture field. Analogous methods are already in use for down-scaling precipitation forecasts based on spectral information [Rebora et al., 2006], and could easily be extended to multifractal descriptions using techniques such as bounded cascade models [Cahalan, 1994].

[19] **Acknowledgments.** This work is part of the second part of the research grant SPP-1294 ‘High Altitude and Long Range Research Aircraft’ (HALO) funded by the Deutsche Forschungsgemeinschaft (DFG). The data set used in this work arises from the DLR Falcon participation in COPS which was supported by the Deutsche Forschungsgemeinschaft (DFG) in the frame of the SPP-1167 ‘Quantitative Precipitation Forecast’.

[20] The Editor thanks the three anonymous reviewers for their assistance in evaluating this paper.

References

- Cahalan, R. F. (1994), Bounded cascade clouds: Albedo and effective thickness, *Nonlinear Processes Geophys.*, *1*, 156–176.
- Cho, J. Y. N., R. E. Newell, and G. W. Sachse (2000), Anomalous scaling of mesoscale tropospheric humidity fluctuations, *Geophys. Res. Lett.*, *27*, 377–380.
- Corrsin, S. (1951), On the spectrum of isotropic temperature fluctuations in an isotropic turbulence, *J. Appl. Phys.*, *22*, 469–473.
- Craig, G. C., and B. G. Cohen (2006), Fluctuations in an equilibrium convective ensemble. Part I: Theoretical formulation, *J. Atmos. Sci.*, *63*, 1996–2004.
- Davis, A., A. Marshak, W. Wiscombe, and R. Cahalan (1994), Multifractal characterizations of nonstationarity and intermittency in geophysical fields: Observed, retrieved, or simulated, *J. Geophys. Res.*, *99*, 8055–8072.
- Emanuel, K. A., and R. T. Pierrehumbert (1996), Microphysical and dynamical control of tropospheric water vapor, in *Clouds, Chemistry and Climate, NATO ASI Ser., Ser. I*, vol. 135, edited by P. J. Crutzen and V. Ramanathan, pp. 17–28, Springer, Berlin.
- Kahn, B. H., et al. (2011), Temperature and water vapor variance scaling in global models: Comparisons to satellite and aircraft data, *J. Atmos. Sci.*, *68*, 2156–2168.
- Kärcher, B., and U. Burkhardt (2008), A cirrus cloud scheme for general circulation models, *Q. J. R. Meteorol. Soc.*, *134*, 1439–1461.
- Kiemle, C., G. Ehret, A. Giez, K. J. Davis, D. H. Lenschow, and S. P. Oncley (1997), Estimation of boundary layer humidity fluxes and statistics from airborne differential absorption lidar (DIAL), *J. Geophys. Res.*, *102*, 189–29,203.
- Kiemle, C., M. Wirth, A. Fix, S. Rahm, U. Corsmeier, and P. Di Girolamo (2011), Latent heat flux measurements over complex terrain by airborne water vapour and wind lidars, *Q. J. R. Meteorol. Soc.*, *137*, 190–203.
- Lewis, G. M., P. H. Austin, and M. Szczodrak (2004), Spatial statistics of marine boundary layer clouds, *J. Geophys. Res.*, *109*, D04104, doi:10.1029/2003JD003742.
- Marshak, A., A. Davis, W. Wiscombe, and R. Cahalan (1997), Scale invariance in liquid water distributions in marine stratocumulus. Part II: Multifractal properties and intermittency issues, *J. Atmos. Sci.*, *54*, 1423–1444.
- Nastrom, G. D., W. H. Jasperson, and K. S. Gage (1986), Horizontal spectra of atmospheric tracers measured during the global atmospheric sampling program, *J. Geophys. Res.*, *91*, 13,201–13,209.
- Obukhov, A. M. (1949), Structure of the temperature field in a turbulent flow, *Izv. Akad. Nauk SSSR Geogr. Geophys.*, *13*, 58–69.
- Pierrehumbert, R. T. (1996), Anomalous scaling of high cloud variability in the tropical Pacific, *Geophys. Res. Lett.*, *23*, 1095–1098.
- Plant, R. S., and G. C. Craig (2008), Parameterization for deep convection based on equilibrium statistics, *J. Atmos. Sci.*, *65*, 87–105.
- Pressel, K. G., W. D. Collins, and A. R. Desai (2010), Variance scaling in water vapor measurements from a tall tower, Abstract P1.77 presented at 13th Conference on Cloud Physics, Am. Meteorol. Soc., Portland, Oreg., 28 June–2 July.
- Rebora, N., L. Ferraris, J. von Hardenberg, and A. Provenzale (2006), RainFARM: Rainfall downscaling by a filtered autoregressive model, *J. Hydrometeorol.*, *7*, 724–738.
- Schaefer, A., A. Doernbrack, C. Kiemle, S. Rahm, and M. Wirth (2010), Tropospheric water vapor transport as determined from airborne lidar measurements, *J. Atmos. Oceanic Technol.*, *27*, 2017–2030.
- Sherwood, S. C., R. Roca, T. M. Weckwerth, and N. G. Andronova (2010), Tropospheric water vapor, convection, and climate, *Rev. Geophys.*, *48*, RG2001, doi:10.1029/2009RG000301.
- Shraiman, B. I., and E. D. Siggia (2000), Scalar turbulence, *Nature*, *405*, 639–646.
- Tompkins, A. M., and J. Berner (2008), A stochastic convective approach to account for model uncertainty due to unresolved humidity variability, *J. Geophys. Res.*, *113*, D18101, doi:10.1029/2007JD009284.
- Tuck, A. F., S. J. Hovde, E. C. Richard, D. W. Fahey, R. S. Gao, and T. P. Bui (2003), A scaling analysis of ER-2 data in the inner Arctic vortex during January–March 2000, *J. Geophys. Res.*, *108*(D5), 8306, doi:10.1029/2001JD000879.
- Vallis, G. K., G. J. Shutts, and M. E. B. Gray (1996), Balanced mesoscale motion and stratified turbulence forced by convection, *Q. J. R. Meteorol. Soc.*, *123*, 1621–1652.
- Xu, Y., L. L. Fu, and R. Tullloch (2011), The global characteristics of the wavenumber spectrum of ocean surface wind, *J. Phys. Oceanogr.*, *41*, 1576–1582.
- Zhang, F., C. Snyder, and R. Rotunno (2003), Effects of moist convection on mesoscale predictability, *J. Atmos. Sci.*, *60*, 1173–1185.
- Zilberman, A., E. Golbraikh, N. S. Kopeika, A. Virtser, I. Kupershmidt, and Y. Shtemler (2008), Lidar study of aerosol turbulence characteristics in the troposphere: Kolmogorov and non-Kolmogorov turbulence, *Atmos. Res.*, *88*, 66–77.

G. C. Craig and L. Fischer, Meteorologisches Institut, Ludwigs-Maximilians Universität, Theresienstrasse 37, D-80333 München, Germany. (george.craig@lmu.de; lucas.fischer@lmu.de)

C. Kiemle, Deutsches Zentrum für Luft- und Raumfahrt, Institut für Physik der Atmosphäre, Münchner Strasse 20, D-82234 Oberpfaffenhofen, Germany. (christoph.kiemle@dlr.de)